ACTIVE PROCESSES ON THE SUN AND THEIR GEOEFFECTIVENESS

Porfir'eva G. and Yakunina G.
Moscow University, Sternberg Astronomical Institute, Moscow, Russia

Abstract. Results of observations during last decades are revised to analyze relations between properties of flares and of Coronal Mass Ejections (CMEs) accompanied by geomagnetic storms. The more massive, quick and wide CMEs are statistically associated with the energetic flares. Solar Proton Events (SPEs) happen often in active regions (ARs) with γβδ magnetic configuration causing extra-ordinary flare activity. The greater area of the AR is the stronger flares and geomagnetic storms are. Influence of variations of direction and velocity of a CME, propagating through the heliosphere, on its geoeffectiveness is discussed. Some aspects of the influence of the flares on the properties of the Earth ionosphere are considered.

Introduction

Heliospheric and geomagnetic disturbances are believed to be mainly caused by solar Coronal Mass Ejections and Solar Energetic Particles (SEPs) events. CMEs origins are due to magnetic reconnection in low corona and accompanied by global reconstruction of magnetic field and can occur in association with solar flares, filament eruptions and streamer ejections. Temporally and spatially related CME and flare, arising from common active region (AR), is considered to be an associated CME/flare. Solar plasma ejections have a great influence on the space weather and can cause strong magnetic storms on the Earth. The strength of the storm depends on many factors, and simple one-to one relation between the flare strength and its geoeffectiveness is not observed but there exist statistical relations between properties of CMEs and associated ARs. Results of observations of CMEs velocity, acceleration, mass, angular width, their propagation through the interplanetary space, influence of magnetic field structure, obtained during last decades, are considered. The variation of the CMEs parameters during their propagation in the corona can significantly influence the CMEs geoeffectiveness.

Relations between properties of CMEs and associated flares

Detailed analysis of data of observations obtained during 1996-2006 was fulfilled by Aarnio et al. [Aarnio et al., 2011]. They used the NASA CME catalog based on white-light observations with the LASCO (Large Angle Spectroscopic Coronograph) aboard SOHO (Solar and Heliospheric Observatory) and GOES (Geostationary Operational Environmental Satellite) flare database. In this period 13,862 identified CMEs and 22,674 flares were registered among which there were 6,733 CMEs with measured mass, width and velocity and 12,050 flares with known heliographic coordinates. Using the criteria for CME-

flare temporal separation (10^m – 80^m) and position angular difference (±45°) 826 associated CMEs/flares pares have been chosen.

Statistically CME mass increases with flare flux:

$$\log M_{CME} = (18.5 \pm 0.27) \times 0.70 \log F_{fl},$$

where the mass of an CME M_{CME} is in *g* and the flare flux F_{fl} is in *Watt* m^{-2}.

Table 1.

Flare class	CME width, °
B	42 ± 4
C	53 ± 0.9
M	63 ± 1.8
X	80 ± 10

CME width increases with CME mass and with the associated flare energy as it can be seen from Table 1, composed by us using the results, presented in Fig. 12 [Aarnio et al., 2011].

The CMEs accompanied by flares have higher velocities (average velocity V_{av} = 495 ± 8 km s^{-1}) than the CMEs not associated with flares (V_{av} = 422 ± 3 km s^{-1}) [Aarnio et al., 2011]. Relation between CME velocity and flare flux is presented in Fig. 1 composed by us using the data from [Zhang et al., 2001; Moon et al., 2003; Zhang et al., 2004; Kumar et al., 2010; Porfir'eva, Yakunina, Oreshina, 2010]. The results by Arnio et al. [2011] agree well with the results presented in [Andrews, 2003; Kuznetsov, 2008; Yashiro et al., 2008].

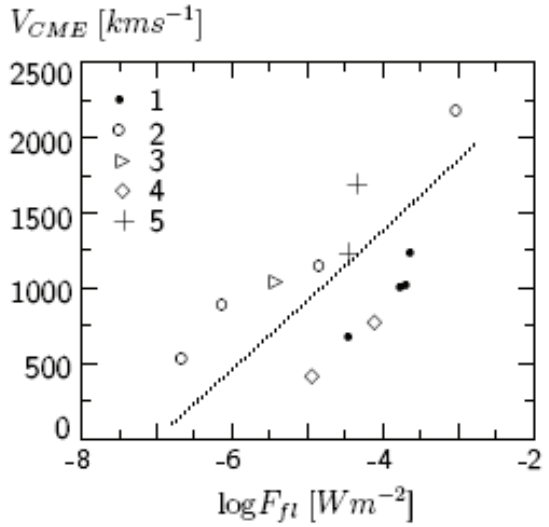

Fig. 1. Relation between observed velocities *V* in *km* s^{-1} and fluxes of associated flares *F* in *W* cm^{-2}:
1 – four CMEs on 1997.11.24-25 AR NOAA 9286;
2 – four CMEs on 1997.01.16, 1997.01.23, 1998.06.11 and 1997.11.06 in the order of increasing velocities V;
3 – CME on 2000.10.25;
4 – two CMEs on 2003.11.20 AR NOAA 10501;
5 – two CMEs on 2003.10.18. AR NOAA 10484 .

Proton events and super-active regions

Proton flux is believed to play an important role in producing geomagnetic storms. Strong proton events often occur in ARs being large δ-islands, when umbrae of opposite magnetic polarities are immersed in common penumbra [Künzel, 1960; Warwick, 1966] or having βγδ magnetic configuration. Such ARs are super-active ones. In Table 2 data on NOAA, date (day.month.year/time of flare maximum), X-ray flare importance/optic class, heliographic coordinates, proton flux F_p, time of proton flux start and geomagnetic

index A_p, that is the index for evaluating the strength of the magnetic field disturbance on the Earth, are presented (see also [Porfir'eva, Yakunina, Delone, 2003] where flares and proton events are considered). A_p-index is measured from a set of standard geophysical stations. A storm begins if $A_p > 29$. The storms with $50 < A_p < 100$ are considered as strong ones. We can see that there is no simple relation between flare strength, proton flux and A_p index. So for the flare X6 (S12E15) on 1991 October 27 F_p is 40 and A_p is 32 and for the weaker flare M7 (S12E15) on 1992 May 8 F_p is 4600 and A_p is 95 although both they occurred near the eastern solar limb. The influence of flares and energetic proton fluxes on the ionosphere of the Earth will be discussed later.

Table 2.

AR NOAA	Date/ UT- day.month.year/ UT	Flare Class	Location	Fp, pfu	Start Day/UT	Ap-index
5395	6.03.1989/ 1405	X15/3B	N35E69	3500	08.03/ 1735	250
5395	17.03.1989/ 1744	X6/2B	N33W60	2000	17.03/ 1855	80
5629	12.08.1989/ 1427	X2/2B	S16W37	9200	12.08/ 1600	73
5698	29.09.1989/ 1133	X9.8	S26W90	4500	29.09/ 1205	153
5747	19.10.1989/ 1258	X13/4B	S27E10	40000	19.10/ 1305	110
5800	30.11.1989/ 1229	X2/3B	N26W59	7300	30.11/ 1345	165
6555	22.03. 1991/ 2247	X9/3B	S26E28	43000	23.03/ 0820	196
6659	04.06.1991/ 0352	X12/3B	N30W70	3000	04.06/ 0820	135
6659	15.06.1991/ 0821	X12/3B	N33W69	1400	14.06/ 2340	130
6703	07.07.1991/0223	X1.9/2B	N26E03	2300	07.07/0455	180
6891	27.10/1991/0548	X6/3B	S12E15	40	28.10/1300	32
6891	30.10.1991/0634	X2/3B	S08W25	94	30.10/0745	
7154	08.05.1992/1546	M7/4B	S26E08	4600	09.05/2045	95
7205	25.06.1992/2014	X3/2B	N09W67	390	25.06/2045	164
7321	30.10.1992/1816	X1,7/2B	S22W61	2700	30.10/1920	32
7671	20.02.1994/0141	M4/3B	N09W02	10000	20.02/0300	95
9077	14.07. 2000/ 1024	X5/3B	N22W07	24000	14.07/1045	164
9393	02.04.2001/2151	X20/	N14W827	1110	02.04/2340	192

In [Tian et al, 2002] 29 ARs existing during 22 and 23 solar cycles are considered. Some parameters were used to describe their activity: XRI is the X-ray flare index evaluating the sum of the flares, multiplied on their importance, the largest area S μh, 10,7 cm peak flux, proton flux F_p and geomagnetic index A_p. We present the results, given in Table 1 and Table 2 by Tian et al. [Tian et al., 2002], as diagrams in Fig. 2 and Fig. 3 (see also Fig. 2–4 in [Porfir'eva, Yakunina, Delone, 2006]). You can see that the larger the area of the AR is, the higher the X-ray flare index is and the higher geomagnetic index Ap is. However by their geoeffectiveness the large and middle ARs differ only slightly. We see that compact ARs can cause the severe storms. The values for large ARs with

S > 1000 μh are presented by red-colored symbols and for the ARs with S < 1000 μh by blue-colored ones.

To describe the magnetic structure of an AR two parameters are used. The tilt angle φ between the axis, connecting the leading and following magnetic polarities in the AR, and solar equator defines the general AR orientation. The free-force parameter α shows magnetic field non-potentiality and delineates how magnetic lines turn around the axis of the flux tube. The active regions tilts can be explained by action of Coriolis force on rising expanding magnetic tubes in the ARs. Accordingly numerous investigations, for typical ARs $|\varphi| < (30°–40°)$, $|\alpha| < 0.02 \times 10^{-6}$ m^{-1} [Bao et al., 2000; Fisher et al., 2000; Linton et al., 1996; Pevtsov et al., 1994; Tian et al., 2002; Tian et al., 2001; Tian et al., 1999] and what's more $\varphi < 0$ for southern ARs, $\varphi > 0$ for northern ARs, and the value depends from the AR heliographic latitude. The ARs usually obey the Hale-Nicholson's and Joy's lows. Observations show that the parameter α is mainly negative in the northern hemisphere and positive in the southern hemisphere independently of the solar cycle.

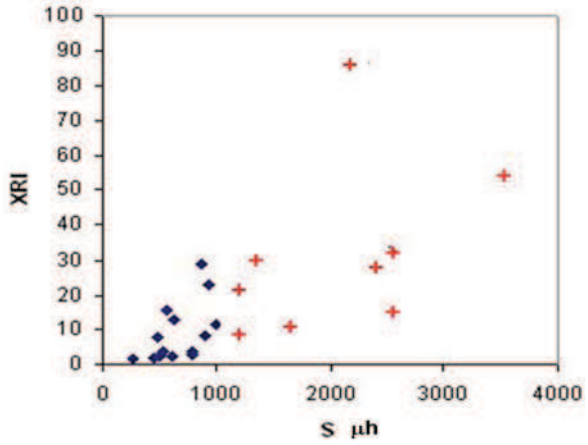

Fig. 2. Relation between the X-ray flare index XRI and spot area S for large (+) and mean (♦) super-active ARs.

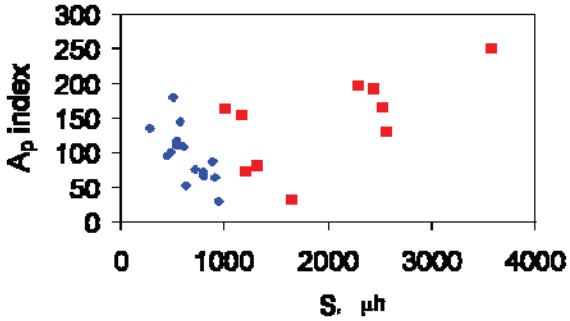

Fig. 3. Relation between geomagnetic index Ap and spot area for large (■) and middle (♦) ARs.

By their properties super-active ARs stand out among other ARs. They have larger areas S, produce stronger flares, more energetic proton fluxes and CMEs. Their tilt angles $|\varphi| > (30°–40°)$ and parameter $|\alpha| > 0.02 \times 10^{-6}$ m^{-1}, as we can see, for example, from the diagrams shown in Fig. 1 [Porfir'eva, Yakunina, Delone, 2004].

Magnetic helicity and coronal mass ejections

The magnetic helicity, characterized by the parameter α, is known to be inhomogeneous and changeable inside the AR area. The flare activity is related with the magnetic helicity and its changes. Statistically preflare helicity of the ARs (and overlying corona), producing strong flares not accompanied by CMEs, is smaller than the helicity of the ARs, producing CME-associated big flares, as it has been shown by Nindos and Andrews [Nindos and Andrews, Ap. J., 2004] who analyzed 133 events occurred during 1966-1999, from which 78 events were associated with big flares. They found that $\alpha=0.018 \pm 0.010$ Mm^{-1} for the ARs with flares not accompanied by CMEs and $\alpha=0.035 \pm 0.018$ Mm^{-1} for the second type ARs, in which associated CMEs-flares were observed.

Latitudinal and longitudinal deflection of CMEs

Observations aboard LASCO SOHO give information in the nearest heliosphere up to distances of 20–30 R_{sun}. Variations of velocity and direction of propagation of a CME play an important role if the CME will rich the Earth, and if it will, then when. At the solar minimum, when the general magnetic field of the Sun might be considered to be approximately a simple dipole, CMEs deflections in latitudinal and longitudinal directions are easier revealed. Particularly the slow CMEs have difficulties to overcome straining forces of overlying magnetic field, they obey polar magnetic field of the Sun, i.e. CMEs tend to propagate from regions with high magnetic energy density to sites of lower magnetic energy density near heliographic current layer. Analogically, inhomogeneities in longitudinal magnetic field strength might cause a deflection of a CME in azimuthal direction to the east or to the west in dependence of the concrete magnetic field structure, as it is discussed in [Shen et al., 2011]. At early stage a CME may deflect for 20–30° from high latitudes toward the solar equator, as for the case of the slow gradually accelerated CME on 8 October 2007 [Shen et al., 2011; Wang et al., 2009]. Propagating in the FOV of the COR1 STEREO B the CME continuously deflected toward the ecliptic plane from the PA (position angle) ~ 306° to PA ~ 276° and beyond 5.5 R_s in the COR2 FOV (field of view) it propagated almost radially. The difference images of the CME for three time moments are presented in Fig. 4, where **a** is for 11:51 – 11:21 UT, **b** for 13:11 – 12:41 UT, and **c** for14:31 – 14:01 UT (in color version: yellow line – radial direction, red lines – CME angular width, blue line – direction of shock wave). The CME showed a helical structure, and Wang et al. [2009] supposed that the CME was seen along its axis and the observed images were cross sections of the helical rope. Similar slow deflected CME on 8 November 2008 was studied by Kilpua et al. [2009].

Earlier the CMEs deflection in the meridian plane was investigated for example using the observations on Skylab during 1972 and 1974 in [MacQueen et al., 1986]. The average deflection toward the ecliptic plane of ~ 2.2° was found. In [Cremades, Bothmer, 2004; Cremades et al, 2006] 124 structured flux-rope

CMEs with known information on the associated source regions (SRs) were analyzed. The observations with the LASCO, EIT, MDI SOHO and base-ground Hα images during 1996–2002 were used. The SR is the active region, where the CME originated. The SRs regions were identified by pre- and post-eruptive events, such as prominences, expanding loops and dimming. The position angle PA of an AR (or a flare) was calculated from its heliographic coordinates. Spatial and temporal coincidence between the CME and its SR was necessary. Comparing the positions angles (PAs) of the CMEs and SRs the authors found that during 1996–1998 (near minimum) the central PAs of the structured CMEs deflected for about 20° to lower latitudes toward the solar equator. At times of the high activity (1999–2002) the deviations, ranging from several degrees to 20°–40°, fluctuated towards the solar poles or equator without a systematical trend (see Fig. 3 in [Cremades et al, 2006]).

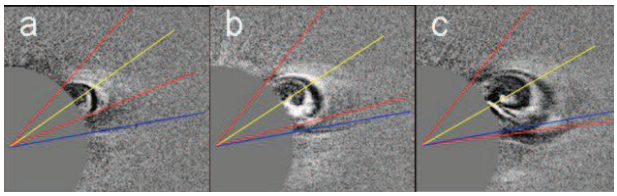

Fig. 4. (Color version online). Deflected slow CME on 2007 October 8 by COR1 STEREO B (based on Fig. 1 from [Shen et al., 2011]).

Yashiro et al. [2008] investigated spatial relation between associated flares and CMSs comparing their PAs. For 1996-2005 LASCO SOHO observations they found 496 flare-CME pairs considering limb events. They concluded that differences between flare PAs and CME central PAs were of ~17°.

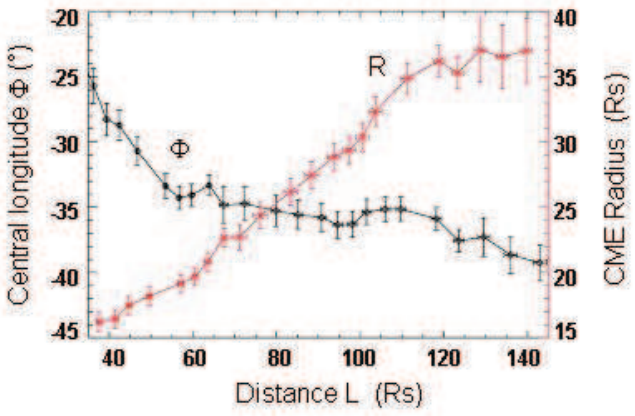

Fig. 5. Evolution of central longitude Φ (black curve) and radius R (*red curve*) of the CME on 2008 April 26 with the distance according to Fig. 3 from [Lugaz et al., 2010], color version on line.

The simultaneous observations in white-light from different view-points in space, made with the wide-angle imagers HI-1 and HI-2 aboard STEREO A and B, give a possibility to follow a CME remotely from the Sun almost to the Earth and to derive the CME shape and the direction of its propagation through the heliosphere. Deflection in longitudinal direction was analyzed by Lugaz et al. [2010], by Liu et al. [2010]. The observations have shown that CMEs (or their pieces) might deflect monotonically or with some temporal fluctuations toward the east (in some cases) or toward the west (in other cases) for about 5°–30° up

to the heliocentric distances of 100–150 R_s. In Fig. 5 the evolution of central longitude Φ (the angle between direction Sun – Earth and direction of propagation of the CME) and radius R of the expanding CME on 2008 April 26 with distance is demonstrated.

The CME propagated to the east from the direction Sun-Earth and its deflection increases for more than 25° when the CME was moving away from the distance of 20 R_s (Φ = –11°) to the distance of 130 R_s (Φ = –37°) . The result agrees well with Φ = –11° by Thernisien et al. [2009] and Φ = –28° by Wood et all [2009].The velocity of the CME was determined to be equal to 534 km s^{-1} and the arrival time to STEREO B was predicted in [Lugaz et al., 2010] with the error of ~11^h.

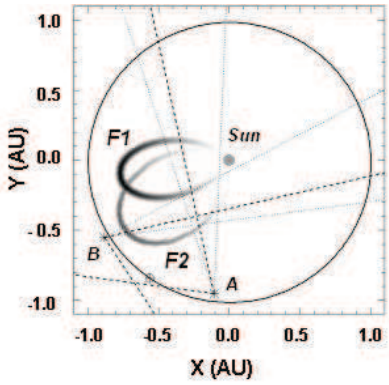

Fig. 6. The location of the fronts F1 and F2 of the CME on 2008 May 17-18, by Fig.1 from [Wood, Howard et al., 2009]. FOVs of the HI1 and HI2 are shown.

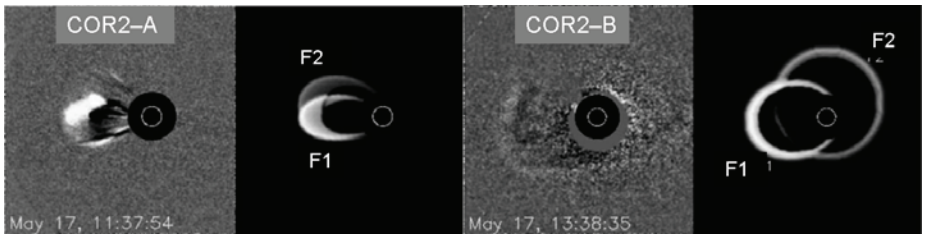

Fig. 7. The STEREO COR2–A and COR2–B images and synthetic images of the CME on 17 May 2008 according to 3D reconstruction, (by Fig.3 from [Wood, Howard et al., 2009]).

Wood et al. [2009] modeled the appearance of the CME on 2008 May 17 by a combination of two expanding fronts F1 and F2. The CME was very fast for the solar minimum and its velocity reached ~1120 km c^{-1}. A slice through the ecliptic plane of 3D model of the CME is shown in Fig. 6. The locations of the Sun and STEREO A and B on the heliocentric coordinates XY are seen. The front F1 was oriented ~2° south the ecliptic and ~52° to the east from the direction Sun – Earth. The front F2 was ~8° north and ~26° to the east from the direction Sun – Earth. Their ecliptic coordinates longitude *l* and latitude *b* were for F1 *l* = 188°, *b* = -2°, and for F2 *l* = 213°, *b* = 8°. The results agree well with the trajectory, defined by Thernisien et al. [2009] who used a flux rope fitting [Thernisien et al., 2006]. The F2 moved almost radially, toward the STEREO B, corresponding the position angle of the B1.7 flare in the center of the solar disc, and the F1 deflected for ~26° as compared with the direction of the F2 and

moved away from both STEREO A and STEREO B. The STEREO A and B and corresponding simulated images at 11:37:54 UT and 13:38:35 UT are shown in Fig. 7.

Solar Proton Events and changes in the Earth ionosphere

In this section we will discuss some aspects of the influence of solar flares, accompanied by proton fluxes, on the structure of the D region in the Earth ionosphere. The conditions in the D region, locating in undisturbed state at the heights from 50 km to 90 km, are important for the propagation of the radio waves on the Earth. Between the lower D region and the oceans (and ground) the Earth-ionosphere waveguide is formed in which the mean frequencies (3 – 30 kHz) propagate usually without interference, going round the Earth globe and causing Schuman resonance (SR) phenomenon. Undergoing multiple reflections between the Earth surface and lower boundary of the ionosphere D region, SR waves give rise to a set of resonance lines. Properties of the D region influence on intensity, amplitude and phase of the radio waves. Energetic particles can produce additional ionization in the lower D region and perturb its upper boundary. Changes in the D region are characterized by two parameters: the reflection height *H'* and the sharpness factor β, that is a measure of the rate of change of the electron density with height in km^{-1}.

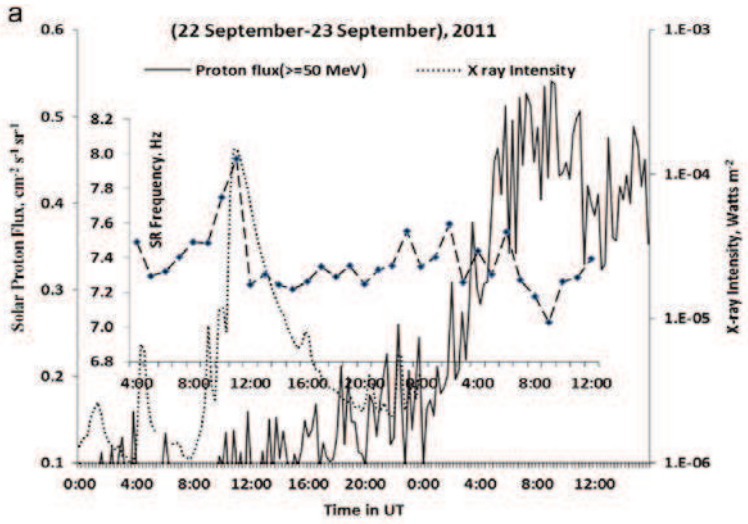

Fig. 8. Relations between the X-ray intensity of the X1 flare on 2011 September 22, proton flux and changes in SR frequency (by Fig. 3a from [Singh, B et al., 2014].

In [Singh, B. et al., 2014] influence of the flares with the SEP on the structure of the D region is analyzed. On the low latitude station near Agra (φ = 14°55′ India) the 19.8 kHz emission, transmitted by the NWC-transmitter from Australia, was registered during the flare X1.4/2N on 2011 September 22 (NOAA 11302, N11E74, flare peak at 10:29 – 11:01 UT, start of the SPE on September 23 at 02:00 UT, maximum at 22:25 UT, duration ~36^h) and the flare X1.1 on 2012 July 6 (NOAA 11515, S18W50, flare peak at 23:01 – 23:08 UT, start of the SPE on July 7 at 00:00 UT, maximum at 07:45 UT, duration 10^h). Event on 2011 September 22 is presented in Fig. 8.

We can see that the proton SR frequency increases for 8,4% during the flare and later decreases for 4,35 %, when the proton flux is peaked. Analogical changes occurred during the flare and following proton flux on 2012 July 6–7. The results can be interpreted by the model accounting for a growth of ionization in the upper part of D region due to the X-ray flare burst and high ionization in the lower D region (at 50–60 km) in the polar region during the SPE. In [Singh A. K., et al, 2014] 32 flares happened during 2011–2012 are analyzed using registration of the 19.8 k Hz emission, transmitted from Australia. Analyzing the changes of the amplitude of the signal, values of H' and β, corresponding to flares of different importance were defined. If, for the quiet ionosphere above the equator of the Earth, H'~71 km and $\beta \sim 0.43$ km^{-1}, during flares 65 km < H'< 70.6 km and $0.433 < \beta < 0.470$ km s^{-1} in dependence of the flare importance. The electron density N_e in the D region can increase in several times. So during the flare M5 on 2012 August 18 N_e increases in the ionosphere above the Earth equator for 320 %.

Summary

Results of the observations of flares and active processes, accompanied by geomagnetic disturbances and happened during the last dozens of the years, are considered. Some statistical relations between the properties of the flares, CMEs and magnetic disturbances characteristics are discussed. The flare is stronger, the mass of the associated CME is bigger: $\log M_{CME} \sim 0.7 \times \log F_{fl}$. The widths of the CMEs, associated with the flares, are statistically proportional to the energetic flare flux and equal to 80° ± 10°, 63° ±1.8° и 42° ± 1.4° corresponding to the X, M and B classes. The CMEs, associated with the flares, rich greater velocities than not associated ones. Their averaged velocities are 495 ± 8 km s^{-1} and 422 ± 3 km s^{-1} respectively.

Energetic proton events occur often in the ARs with δ or βγδ-magnetic configuration. For such ARs the area is larger the X-ray flare index is higher and geomagnetic index A_p is greater.

The problem of the propagation of CME through the heliosphere is discussed. Changes in the velocity and direction are important and define if the CME approach the Earth and when. The influence of flares and SPEs on the properties of the D region of the ionosphere is considered. During the flares the reflecting region height (above the surface of the Earth) decreases and N_e inside it increases, associated with the flares

References

Aarnio, A.N., Stassun, K.G., Hughes, W.J., and McGregor, S.L. Solar Phys. **268**, 195, 2011.
Andrews M. D., Solar Phys, **218**, 261, 2003.
Bao S.D., Pevtsov A.A., Wang T.J., Zhang H.Q., Solar Phys. **195**, 75, 2000.
Cremades H., Bothmer V., Tripathi D., Adv. Space Res. **38**, 461, 2006.
Cremades H., Bothmer V., Astron.&Astrophys. **422**, 307, 2004.
Fisher G.H., Fan. Y., Longcope D.W. et al,. Solar Phys. **192**, 119, 2000.